

Observable coherence theory for statistically periodic fields

Brynmor J. Davis*

The Beckman Institute for Advanced Science and Technology, University of Illinois at Urbana-Champaign, Urbana, Illinois 61801, USA

(Received 25 July 2007; published 30 October 2007)

The framework of cyclostationary random processes is used to develop classical coherence theory for the measurement of statistically periodic stochastic optical fields, such as those produced by pulsed lasers. Cycloergodicity is invoked to show that precise and accurate inferences of the nonstationary process statistics can be made from a single field realization. In particular, many-pulse observations using nonlinear and/or nonstationary techniques, such as spectral shearing interferometry, can be used to fully characterize the standard two-time correlation function of a statistically periodic source. The theory is demonstrated through the simulation of spectral shearing interferometry and frequency-resolved optical gating measurements.

DOI: [10.1103/PhysRevA.76.043843](https://doi.org/10.1103/PhysRevA.76.043843)

PACS number(s): 42.25.Kb, 42.60.Mi, 42.65.Re

I. INTRODUCTION

Coherence theory [1–3] is a response to two important observations about the nature of optical measurements. First, detector limitations will generally preclude the direct inference of a complex electromagnetic field, giving instead only time-integrated intensity measurements. Second, optical fields are generally stochastic due to imperfect knowledge of the optical source and/or the inherently probabilistic nature of the generation of light. The resulting framework makes coherence theory indispensable in the prediction of observable optical phenomena. As noted in Ref. [4], “An interesting feature of the theory of coherence is that it operates with measurable quantities only.”

Considering photodetector sensitivity and response times, it is clear that the set of observable measurements is much smaller than the set of physically allowable source statistics. As coherence theory describes quantities measurable by such real instruments, the set of fields to which it can be applied is necessarily restricted. The restrictions most commonly enforced are those of stationarity and ergodicity. Stationarity requires that the ensemble statistics of the field do not vary with time, and ergodicity ensures that a time-averaged detector response can be expected to converge to the appropriate ensemble probabilistic measure. While stationarity and ergodicity cannot hold for causal fields or finite-time measurements [5,6], they provide sufficiently accurate approximate models for real-world signals in a wide variety of important cases. Indeed coherence theory can be used to describe and understand many interesting optical phenomena occurring with nondeterministic light or stochastic optical systems—e.g., propagation-induced spectral changes [7], white light interference [8], atmospheric beam wander [9], etc. Additionally, an understanding of coherence theory forms the basis of many instruments that use the statistical nature of light to make inferences—e.g., stellar speckle interferometry [10], optical coherence tomography [11], interference spectroscopy [12,13], etc. In short, coherence theory is used to make sense of observable data.

While stationarity and ergodicity are of great utility in the interpretation of optical measurements, stochastic nonsta-

tionary fields are increasingly important in modern optics, particularly with the expanding use of pulsed laser sources and the ever-increasing speed of those sources. Although nonstationary coherence theory is less mature than stationary coherence theory, it is the subject of a significant body of literature. For example, it has been shown that physical considerations impose certain laws on the allowable space-time correlations of a nonstationary electromagnetic field [14,15] and nonstationary-field propagation in certain systems can be analyzed [16–19]. One may also define a nonstationary modal decomposition [20,21] analogous to the coherent-mode decomposition. Authors have posited various restrictions on the statistics of the field in order to define tractable classes of nonstationary fields. For example, in the elementary pulse model a field is constructed as an incoherent sum of temporally distinct, fully coherent pulses [22]; the dual of this model, the spectral elementary pulse model, has also been described [23]; alternatively, an intrinsically stationary field [6,24,25] consists of a stationary source that is temporally modulated. Such nonstationary models are typically defined in terms of correlation functions—i.e., ensemble moments of the field. Consequently, it may be possible to determine the ensemble expectation of a hypothetical instantaneous measurement or of a time-integrated quantity. However, without ergodicity (which is usually taken to imply stationarity; e.g. see Ref. [26], Sec. 12-1), there is no guarantee that a time-integrated measurement from a single field realization will converge to the calculated ensemble expectation. For the statistically periodic (cyclostationary) fields considered here, convergence can be guaranteed under certain cycloergodicity conditions. Restated, the statistics of cycloergodic fields may be estimated in an accurate and precise manner, but precision cannot be guaranteed for arbitrary nonstationary fields.

This work leverages the well-developed field of cyclostationary random processes in an analysis of the metrology of nonstationary fields. An overview of cyclostationarity can be found in Ref. [27], while Ref. [28] contains a comprehensive bibliography of publications concerning cyclostationarity. Cycloergodicity is invoked to allow the measurement of statistically stable time-integrated measurements from nonstationary fields. As with standard ergodic coherence theory, the cycloergodic coherence theory described here is only applicable to a subset of the set of arbitrary fields; however, this

*bryn@uiuc.edu

subset is substantially larger than the standard ergodic set. Cyclostationarity requires that the ensemble statistics of the field be periodic in time, as opposed to stationarity which requires that they be constant in time. Cyclostationarity has been mentioned in relation to optical fields in the literature [29–32] but its potential for optical metrology has not been fully exploited. This is in contrast to other fields where cyclostationarity has been heavily utilized, including in optical signal processing [33].

The pulsed fields produced by modelocked or Q -switched lasers are becoming increasingly important in laboratory settings. In addition, pulsed lasers are being used in conjunction with nonlinear systems to produce novel sources—e.g., extreme ultraviolet or soft x-ray pulse trains [34,35], terahertz (THz) fields [36,37], and broadband continua [38]. Cyclostationarity is a natural model for these sources as they can be expected to exhibit periodic statistics. The work presented here allows the statistical interpretation of measurements taken from such sources, with the goal of allowing measurement-based inference of the source statistics. The statistical behavior of the source determines the temporal and spectral distribution of energy, the stability of the field, and the potential efficacy of techniques such as optical pulse compression [39]. Preliminary work in the measurement of broadband continua has already shown interesting statistical phenomena and significant pulse-to-pulse instability [40]. It will be shown that instruments designed to provide deterministic single-pulse characterization, such as spectral phase interferometry for direct electric-field reconstruction (SPIDER) [41,42] and frequency resolved optical gating (FROG) [43,44], can also be used to provide a statistical characterization of periodically pulsed fields by taking many-pulse measurements.

The next section provides a terse review of cyclostationary random processes and establishes the notation. In Sec. III cycloergodicity is briefly reviewed and consistent estimators of the second-order correlations of a cycloergodic random process are described. The stable measurement of periodic field statistics is discussed in Sec. IV with SPIDER and FROG examples given. Many-pulse SPIDER and FROG results are simulated in Sec. V and are shown to agree with theoretical predictions. A discussion and references conclude this work.

II. CYCLOSTATIONARITY

The coherence theory presented in this paper hinges on the assumption of the cyclostationarity of the stochastic fields in question. A cyclostationary model is chosen for two reasons: it is a natural framework in which to analyze stochastic periodically pulsed fields, and it allows the invocation of cycloergodicity to interpret measurements in terms of the ensemble statistics of the field. Cyclostationary stochastic processes have been extensively studied, and the reader is referred to the literature (see Refs. [27,28]) for a comprehensive discussion. A limited review is given here in order to lay the groundwork for the optics-centered results presented later in the paper.

A. Definition

Here and in the rest of this work, the notation of Ref. [2] is followed when applicable. In particular, the temporal Fourier transform operator is defined as $\int \exp[i2\pi\nu t]dt$.

Let the complex random process $E(t)$ be the complex analytic envelope of a real scalar field. An n th-order probability density function (PDF) $p(\xi_1, \xi_2, \dots, \xi_n; t_1, t_2, \dots, t_n)$ defines the joint statistics of $E(t)$ at n times; i.e., it describes the probability that E takes value ξ_1 at time t_1 , ξ_2 at time t_2 , etc. To obtain a complete characterization of a general random process, the PDF must be specified to an infinite order. In the stationary case the PDFs obey the equation

$$p(\xi_1, \xi_2, \dots, \xi_n; t_1, t_2, \dots, t_n) = p(\xi_1, \xi_2, \dots, \xi_n; t_1 + T, t_2 + T, \dots, t_n + T), \quad (2.1)$$

for all T . The implication is simply that the statistical characteristics of the random process are not dependent on the origin of the time axis. Cyclostationarity is less restrictive than stationarity—Eq. (2.1) must still be satisfied but only for *some* T . The smallest value of T for which Eq. (2.1) is satisfied is known as the period of the process. The statistical properties of a cyclostationary random process are dependent on the origin of the time axis but this dependence is periodic.

B. Correlations and spectra

It is not usually possible to measure the PDFs that fully characterize a random optical field. For this reason, aggregate properties are typically used to partially characterize the field. The moments of the PDF are a popular metric and are often expressed in terms of correlation functions. Following Ref. [2], the correlation function of order (M, N) is defined as

$$\Gamma^{(M, N)}(t_1, t_2, \dots, t_{M+N}) = \langle E^*(t_1)E^*(t_2) \cdots E^*(t_M)E(t_{M+1}) \cdots E(t_{M+N}) \rangle, \quad (2.2)$$

where $\langle \cdot \rangle$ is the expectation operator.

The correlation functions for which $M=N$ appear most commonly in standard coherence theory. Following Ref. [2], such correlation functions will be referred to as even-order, while correlation functions for which $M \neq N$ are odd-order. Odd-order correlation functions receive little attention because they can be shown to be zero for a stationary source in all but a limited set of special cases (see Ref. [2], Sec. 8.3, for a full discussion). In the nonstationary case the odd-order correlation functions may be nonzero, which implies that a phase shift ϕ changes the statistics of the field. If $E(t)$ is replaced by $e^{i\phi}E(t)$ in Eq. (2.2), it can be seen that the even-order ($M=N$) correlations are unaffected, while the odd-order correlations change. Thus a field with nonzero odd-order correlations has quadrature components with differing statistics; e.g., $\Gamma^{(2,0)}(t_1, t_2)$ can be used to describe squeezed light [45]. In this work it is assumed that all odd-order correlation functions are zero so that the quadrature components are statistically equal, the field is unsqueezed, and there is no preferential phase offset.

Fourier-domain spectral correlations have also found great utility. The Fourier transform of the random process $E(t)$ is denoted by $\tilde{E}(\nu)$ and is assumed to exist, at least in the sense of mean-square stochastic convergence (see Ref. [26], Sec. 11-4). The spectra $\Phi^{(M,N)}$ can then be defined as

$$\begin{aligned} \Phi^{(M,N)}(\nu_1, \nu_2, \dots, \nu_{M+N}) &= \langle \tilde{E}^*(\nu_1) \tilde{E}^*(\nu_2) \cdots \tilde{E}^*(\nu_M) \tilde{E}(\nu_{M+1}) \cdots \tilde{E}(\nu_{M+N}) \rangle, \\ &= \int \cdots \int \Gamma^{(M,N)}(t_1, t_2, \dots, t_{M+N}) \prod_{j=1}^M \exp[-i2\pi\nu_j t_j] \\ &\quad \times \prod_{k=M+1}^{M+N} \exp[i2\pi\nu_k t_k] dt_1 dt_2 \cdots dt_{M+N}. \end{aligned} \quad (2.3)$$

The spectra defined above give a measure of the correlation between frequency components of the field. These spectra facilitate the interpretation of nonstationary optical fields as a composition of correlated spectral components [46,47]. Such an interpretation is particularly apt for modelocked lasers, where the multiple modes generated in the laser cavity ideally have a well-defined intermode phase relation.

Since optical detectors respond to the optical intensity $|E(t)|^2$, the $M=N=1$ correlation function and spectrum are of particular interest. Cyclostationarity can be seen to enforce a particular structure on these functions. Since $\Gamma^{(1,1)}(t_1, t_2) = \Gamma^{(1,1)}(t_1+T, t_2+T)$, a Fourier series expansion can be made as

$$\Gamma^{(1,1)}(t - \tau, t) = \sum_{m=-\infty}^{\infty} C(\tau; m) e^{-i2\pi m \nu_T t}, \quad (2.4)$$

where the repetition frequency is defined as $\nu_T = T^{-1}$ and m is an integer. Using Eq. (2.3), it can then be seen that

$$\Phi^{(1,1)}(\nu, \nu + \mu) = \sum_{m=-\infty}^{\infty} W(\nu; m) \delta(\mu - m\nu_T), \quad (2.5)$$

where

$$W(\nu; m) = \int C(\tau; m) e^{i2\pi\nu\tau} d\tau. \quad (2.6)$$

Cyclostationarity implies that the spectrum $\Phi^{(1,1)}(\nu_1, \nu_2)$ consists of continuous distributions of singularities along lines of unit slope in the $\nu_1 - \nu_2$ plane, herein referred to as δ lines. These δ lines are spaced by multiples of the repetition frequency. This shows that only certain frequency components of the field have correlations. For stationary fields it can be seen that only the $m=0$ term is nonzero in Eq. (2.4). In this case $W(\nu; 0)$ becomes the standard spectral density and frequency components of the field are uncorrelated.

The form seen in Eq. (2.5) clearly places a spectral restriction on the class of nonstationary fields that can be considered. As noted in Sec. I, some restriction is necessary in order to ensure a meaningful relationship between detector measurements and the statistics of the source. Cyclostationarity allows the cycloergodic relations discussed in the next

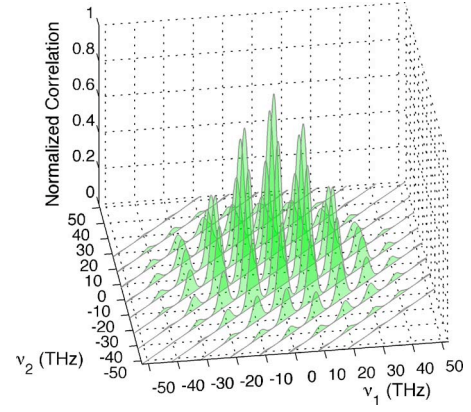


FIG. 1. (Color online) Graphical representation of the spectrum $\Phi_C^{(1,1)}(\nu_1, \nu_2)$ of an example cyclostationary random process. Spectral correlations are nonzero only along lines of unity slope, offset by multiples of the pulse repetition frequency.

section to be employed, while also encompassing a broad class of optical fields encountered in modern optics.

The spectrum of an example cyclostationary random process $E_C(t)$ is illustrated in Fig. 1. In this case a cyclostationary field is created by periodically modulating a stationary field,

$$E_C(t) \propto a(t)E_I(t). \quad (2.7)$$

Nonstationary fields constructed in this manner are known as intrinsically stationary [6]. In this example a periodic Gaussian modulation function is used,

$$a(t) = \sum_{n=-\infty}^{\infty} e^{-(t-nT)^2/(2\sigma_a^2)}, \quad (2.8)$$

with $\sigma_a = 10$ fs and $T = 100$ fs. The underlying stationary field $E_I(t)$ is defined by a Gaussian correlation function

$$\Gamma_I^{(1,1)}(t - \tau, t) = e^{-\tau^2/(2\sigma_I^2)}, \quad (2.9)$$

where $\sigma_I = 100$ fs. The pulse repetition rate T used in this example allows clear visualization of the field spectrum but is much higher than the repetition rate achieved in modern pulsed lasers.

A stationary field $E_S(t)$ with the same spectral content as $E_C(t)$ may be defined by setting $W_S(\nu; 0) = W_C(\nu; 0)$. However, since this field is stationary, $W_S(\nu, m) = 0$ for all $m \neq 0$. The resulting spectrum can be seen in Fig. 2. The cyclostationary field $E_C(t)$ and the stationary field $E_S(t)$ will be used in illustrative examples throughout this work.

A comparison of Figs. 1 and 2 illustrates the differences between the second-order spectrum of a stationary process and that of a cyclostationary process. In Fig. 2, temporal stationarity requires that distinct Fourier components be uncorrelated, with the result that the spectrum is nonzero only on the $\nu_1 = \nu_2$ locus. The less restrictive condition of cyclostationarity allows correlations between Fourier components separated by multiples of ν_T . As a result the spectrum is nonzero along the offset, unity-slope δ lines seen in Fig. 1. This spectrum is more general than the stationary case, but

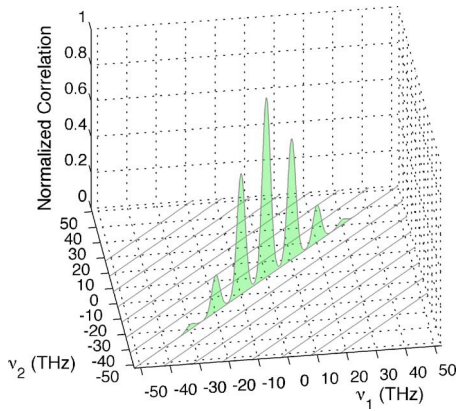


FIG. 2. (Color online) Graphical representation of the spectrum $\Phi_S^{(1,1)}(\nu_1, \nu_2)$ of an example stationary random process. Spectral correlations are nonzero only along the $\nu_1 = \nu_2$ line.

more restrictive than the general nonstationary case where periodic statistics are not required and any two Fourier components may be correlated.

III. CYCLOERGODICITY

A. Motivation

Cycloergodicity can be invoked to relate a single realization of a cyclostationary random process to the probability distributions that define it. Since a single realization of the process is generally all that is experimentally available, cyclostationarity provides an important tool for making inferences about the probabilistic properties of the field. Formally, a cyclostationary process is cycloergodic in some function of the PDF if that function of the PDF can be *consistently* estimated from a single realization of the random process. If $g_L[E(t)]$ estimates the field parameter θ from a duration L measurement of the field $E(t)$, then consistency requires (see Ref. [26], Sec. 8-2),

$$\lim_{L \rightarrow \infty} \mathcal{P}\{|g_L[E(t)] - \theta| < \epsilon\} = 1, \quad (3.1)$$

for all $\epsilon > 0$ and where “ \mathcal{P} ” is probability. In practical experiments a finite observation time is used but is understood to be long enough to allow the estimator to converge to within a reasonable distance of the infinite-observation value. Magyar and Mandel performed a maser experiment where the effects of insufficient measurement duration are demonstrated [48].

In the same manner that ergodicity requires stationarity, cyclostationarity is a necessary, but not sufficient, condition for cycloergodicity. While a description of the conditions necessary for cycloergodicity is beyond the scope of this work, Gardner *et al.* [27] provide the following summary: “Consistent estimates of second-order statistical functions of an [almost cyclostationary] stochastic process can be obtained provided that the stochastic process has finite or ‘effectively finite’ memory. Such a property is generally expressed in terms of mixing conditions or summability of second- and fourth-order cumulants.” Almost-cyclostationary

processes form a broader class than the cyclostationary processes considered here. Intuitively, the periodic nature of the cyclostationary random process allows probabilistic measures to be estimated using an averaging procedure over many periods of a single realization. If the process has an infinite memory, the single realization may not be representative of all possible outcomes, giving a process that is not cycloergodic. For a discussion of this idea in the stationary framework, see Ref. [2], Secs. 2.2.2 and 2.2.3.

In the general nonstationary case there are no constraints on the temporal dependence of the statistics of the field. So while it is possible to define probabilistic measures (such as the mean and higher-order moments) as a function of time, it is not generally possible to consistently predict the outcomes of time-integrated measurements or to infer probabilistic information from such measurements. As an example, consider the estimation of the expected intensity as a function of time for a random field. In the general nonstationary case, a single field realization can give little indication of the time-dependent expected value—at each point in time only a single datum is available. The uncertainty of the expected intensity at a given time is nonzero and may not be reduced by taking more data. A precise estimate of the time-dependent mean intensity cannot be found. In the cycloergodic case, one can perform an averaging across periods of the field in order to get a consistent estimate of the expected intensity at each position within a period.

In general, some restrictions on the nonstationarity of the field are required in order to meaningfully interpret measurements. These restrictions limit the utility of completely general nonstationary coherence theory. In a recent work a statistical description of pulse trains was presented [49] in a manner that allowed the modeling of various effects including pulse-to-pulse correlations. That work implicitly employs a restricted cyclostationary model. As a result, the authors report spectral correlations of the form seen in Eq. (2.5) but cycloergodicity was not exploited. The analyses presented here are based on a less restrictive model and invoke cycloergodicity to allow the prediction of measurements and the use of single field realizations in inferences regarding the probabilistic properties field.

As a caveat, it should be noted that cyclostationarity is not the only nonstationary model that may produce ergodicity properties. For example, a stable, predictable, slow detector measurement may be possible for a field consisting of a slowly varying nonstationary component and a rapidly varying stationary component. This is known as a locally stationary model [5,50] and can be used in situations where the coherence length of a field is much less than the pulse width [25,51,52]. Local stationarity does not apply to stable ultrafast pulse trains, as the field can be expected to remain coherent within a single pulse duration, or even between pulses.

B. Time-frequency correlation estimation

The estimators presented in this section and in Sec. III C represent only a small fraction of the literature on cycloergodicity, and a more comprehensive review is recommended [27,28].

The coefficients $C(\tau; m)$ seen in Eq. (2.4) can be estimated from a single realization of the field $E(t)$ using

$$\hat{C}(\tau; m, l, L) = \frac{1}{L} \int_{l-L/2}^{l+L/2} E^*(t - \tau) E(t) e^{i2\pi m \nu t} dt. \quad (3.2)$$

The estimate \hat{C} is a function of L , the measurement duration, and l , the central time in the measurement. Assuming cycloergodicity, $\hat{C}(\tau; m, l, L)$ is a consistent estimator of $C(\tau; m)$, so that

$$\lim_{L \rightarrow \infty} \langle \hat{C}(\tau; m, l, L) \rangle = C(\tau; m) \quad (3.3)$$

and

$$\lim_{L \rightarrow \infty} \langle |\hat{C}(\tau; m, l, L) - \langle \hat{C}(\tau; m, l, L) \rangle|^2 \rangle = 0. \quad (3.4)$$

It can be seen that these limits are not dependent on the measurement origin l . The mean condition seen in Eq. (3.3) ensures accuracy, while the variance condition of Eq. (3.4) describes precision. Together these two consistency conditions are denoted by \xrightarrow{L} , where the limit is taken with respect to the under-set variable(s). This allows Eqs. (3.3) and (3.4) to be written as

$$\hat{C}(\tau; m, l, L) \xrightarrow{L} C(\tau; m). \quad (3.5)$$

C. Frequency-frequency correlation estimation

The estimator given in Sec. III B is a function of the temporal variable τ and the spectral-offset index m . An estimator can also be implemented entirely in the spectral domain by first defining the intermediate measurement

$$F(\nu; l, L) = \int_{l-L/2}^{l+L/2} E(t) e^{i2\pi \nu t} dt. \quad (3.6)$$

$F(\nu; l, L)$ can be interpreted as a limited-time Fourier transform or, by regarding l as a variable rather than a parameter, a bandpass filter about ν . An estimated spectrum can then be defined as

$$\hat{W}(\nu; m, l', L', L) = \frac{1}{L'} \int_{l'-L'/2}^{l'+L'/2} \frac{1}{L} F^*(\nu; l, L) F(\nu + m\nu_T; l, L) dl, \quad (3.7)$$

where l' defines temporal origin of measurement, L' is the length of measurement, and L^{-1} gives the spectral resolution of $F(\nu; l, L)$. Cycloergodicity can then be invoked to give

$$\hat{W}(\nu; m, l', L', L) \xrightarrow{L, L'} W(\nu; m), \quad (3.8)$$

where the limit in L' is taken before the limit in L . The convergence shown in Eq. (3.8) is predicated on the assumption that $W(\nu; m)$ is a smooth function of ν . In the event that it is not smooth, the estimator converges to a smoothed version of $W(\nu; m)$ (see Ref. [27] for details).

In practical measurements, L' and L cannot achieve the limits in Eqs. (3.5) and (3.8). Instead, these parameters must

be large enough to allow the estimators to converge to within an acceptably small variance. If τ_c is the maximum width of $\Gamma^{(1,1)}(t - \tau, t)$, then the measurement duration has to be many multiples of τ_c or T (whichever is larger). For the remainder of this work it is assumed that these conditions on L and L' are met.

IV. MEASUREMENT OF PULSED FIELDS

In this section the measurement of a field with a cyclostationary envelope $E(t)$ is considered. Consistent with the majority of the nonstationary coherence theory literature, attention is largely restricted to the second-order correlations $\Gamma^{(1,1)}(t_1, t_2)$ or, equivalently, $\Phi^{(1,1)}(\nu_1, \nu_2)$. These functions are insufficient to fully characterize the field but are closely related to data measured in experimental systems. In the stationary case, $\Gamma^{(1,1)}(t_1, t_2)$ [or $\Phi^{(1,1)}(\nu_1, \nu_2)$] characterizes the statistics of the process up to second order. This is also true of the nonstationary case when $\Gamma^{(1,0)} = \Gamma^{(2,0)} = 0$ as assumed here.

The measurement instrumentation is modeled as a detector preceded by optical elements that are used to transform the field in some manner. A slowly responding detector of intensity can be modeled as giving $\hat{C}(0; 0, l, L)$ from Eq. (3.2). Similarly, a spectrometer can be modeled as providing $\hat{W}(\nu; 0, l', L', L)$ [Eq. (3.7)]. The information collected by the intensity detector is a subset of that provided by the spectrometer—i.e., the intensity detector data can be synthesized from the spectrometer measurement but not vice versa. For this reason, spectral detection will be considered throughout this section, with the understanding that it represents the more general detection method.

The spectrometer is modeled as collecting $\hat{W}(\nu; m, l', L', L)$ for $m=0$, which consistently estimates $W(\nu; 0)$ for cycloergodic fields. Thus the spectrometer does not provide an unambiguous characterization of the spectrum $\Phi^{(1,1)}(\nu_1, \nu_2)$ unless the field is stationary, in which case $W(\nu; m)$ is nonzero only for $m=0$. In order to measure the second-order statistics of $E(t)$, the goal is to design predetector optical elements that produce a field that can be used to fully estimate the spectrum of $E(t)$ —i.e., to find $W(\nu; m)$ for all m . As a first step in this design process, one can consider linear, temporally stationary, predetector optics.

A. Stationary linear measurements

A linear, temporally stationary optical system can be characterized by an impulse response $h(t)$. The resulting predetector field envelope is then

$$P(t) \propto h(t) * E(t), \quad (4.1)$$

where $*$ represents convolution. This operation can also be represented in the Fourier domain by the transfer function $\tilde{h}(\nu)$. It should be noted that since $E(t)$ is cyclostationary with period T , $P(t)$ is also cyclostationary with period T .

The data collected by the spectrometer are represented by $D(\nu; l', L', L)$, which is defined according to Eq. (3.7) but where $P(t)$ is measured rather than $E(t)$ and $m=0$.

$D(\nu; l', L', L)$ is a consistent estimator of $W_p(\nu; 0)$, the $\nu_1 = \nu_2$ δ -line coefficients of the spectrum of $P(t)$. The spectrum of $P(t)$, $\Phi_p^{(1,1)}(\nu_1, \nu_2)$, can be related to the spectrum of $E(t)$ using Eq. (4.1) and standard stochastic results. Assuming cycloergodicity, the resulting spectrometer data converge as

$$D(\nu; l', L', L) \xrightarrow{L, L'} W_p(\nu; 0) = |\tilde{h}(\nu)|^2 W(\nu; 0). \quad (4.2)$$

The linear, temporally stationary model includes a number of common instruments. For example, an interferometer can be modeled with the impulse response $h(t) = \delta(t) + \delta(t - \tau)$.

From Eq. (4.2) it can be seen that linear, temporally stationary, predetector optics do not give access to $W(\nu; m)$ for $m \neq 0$. As a result, the instrument is still insensitive to much of the two-frequency spectrum $\Phi^{(1,1)}(\nu_1, \nu_2)$. The inadequacy of linear, temporally stationary measurements in the characterization of pulsed fields has been previously noted in a deterministic context [53,54].

The use of the $\nu_1 = \nu_2$ line of $\Phi^{(1,1)}(\nu_1, \nu_2)$ as an intuitive and accessible spectrum for nonstationary fields has been proposed [55]. As described above, this locus of the two-frequency spectrum does describe the expected value of spectral measurements of $E(t)$, and the measurement may converge to this value for cyclostationary or other well-behaved fields. While such measurements may be predicted, they do not allow the inference of nonstationary statistics. This can be seen by noting that one may always construct a stationary random process with a single-frequency spectrum of $\Phi^{(1,1)}(\nu, \nu)$, as seen in the examples of Figs. 1 and 2. The nonuniqueness of second-order nonstationary fields constrained only by $\Phi^{(1,1)}(\nu, \nu)$ has also been noted in the context of temporally Gaussian pulses [56] and intrinsically stationary fields [25].

Despite such ambiguities, the prevalence of linear, temporally stationary measurement optics has resulted in most stochastic pulsed sources being characterized in terms of the single-frequency spectrum $\Phi^{(1,1)}(\nu, \nu)$. The standard approach is to posit a source model based either on mathematical [22,23,49] or physical [57–59] considerations. Noise and stochastic influences are also modeled (often in terms of concepts such as jitter, pulse-width fluctuation, or carrier-envelope offset) and the ensuing effects on $\Phi^{(1,1)}(\nu, \nu)$ investigated. The resulting explanations of measurements and noise sources are model dependent and subject to significant interpretation difficulties [29].

The approach taken in this work is to make only a limited assumption about the source statistics (i.e., cycloergodicity), to not restrict noise sources, and to measure more data. Specifically, $\Phi^{(1,1)}(\nu_1, \nu_2)$ is estimated for $\nu_1 \neq \nu_2$. In order to do this, nonlinear and/or nonstationary measurement optics must be used. This approach is in line with ultrafast pulse characterization techniques such as SPIDER and FROG, which are inherently nonlinear and/or nonstationary. Ultrafast measurement techniques such as these have been presented in a deterministic framework with the goal of measuring a single, isolated pulse. The stochastic measurement analyzed here differs in that the measurement is taken over many pulses in order to reliably measure statistical quanti-

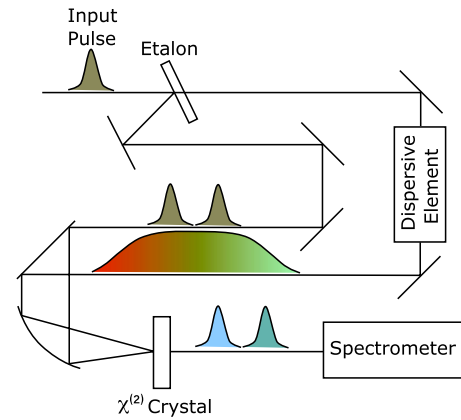


FIG. 3. (Color online) Illustration of the SPIDER pulse measurement technique, where the pulse shading indicates frequency content. An étalon is used to create two offset replicas of the pulse, while a chirped version of the pulse is produced in a dispersive element. These fields are mixed in a nonlinear crystal and the resulting up-converted pulses detected with a spectrometer.

ties. It should also be noted that the assumption of cyclostationarity is less restrictive than most pulsed-source models and that the issue of ergodicity has been largely ignored in previous work on nonstationary optical fields.

B. Spectral-shearing interferometry

The use of nonlinear and/or nonstationary optics to measure cyclostationary signals can be well demonstrated with a SPIDER system. The SPIDER technique is illustrated in Fig. 3 using a diagram based on Fig. 1 in Ref. [60]. The reader is also referred to that article for a discussion of practical issues involved in the construction of the interferometer. The SPIDER apparatus uses a nonlinear crystal to mix two temporally offset replicas of the field $E(t)$ with a third highly dispersed copy. Since the time response of the apparatus is dependent only on the cyclostationary field $E(t)$, the field envelope at the detector, $P(t)$, is cyclostationary. The cycloergodicity of $P(t)$ is also assumed in this work.

Part of the field $E(t)$ is passed through a dispersive element to produce a chirped pulse with a long duration. This dispersed pulse is mixed with each of two temporally offset pulses in a nonlinear $\chi^{(2)}$ crystal. The dispersion introduced is assumed to allow the dispersed pulse to be regarded as a pure frequency across the duration of an undispersed pulse. Each of the undispersed, offset pulses is mixed with a different portion of the dispersed signal and thus mixes with a different frequency. A relative frequency shear μ is produced and the SPIDER signal is modeled as [41]

$$P(t; \tau, \mu) \propto E(t) + E(t - \tau)e^{i2\pi\mu t}, \quad (4.3)$$

where τ gives the temporal offset produced in the étalon seen in Fig. 3. It should be noted that the model given by Eq. (4.3) requires a sufficiently short and well-defined pulse profile. In general, cyclostationary fields need not be restricted to those with periodically localized intensity distributions. Additionally, Eq. (4.3) describes the ideal situation where the dis-

persed pulse behaves as a pair of local oscillators for mixing with each of the offset pulses. In a field with significant random fluctuations this model may not be accurate.

From Eq. (4.3) it can be seen that the Fourier-domain representation of the predetector envelope is

$$\tilde{P}(v; \tau, \mu) = \tilde{E}(v) + \tilde{E}(v + \mu)e^{i2\pi(v+\mu)\tau}. \quad (4.4)$$

The $\nu_1 = \nu_2$ profile of the resulting spectrum is, then,

$$\begin{aligned} \Phi_p^{(1,1)}(v, v; \tau, \mu) &= \langle |\tilde{E}(v)|^2 + |\tilde{E}(v + \mu)|^2 \\ &\quad + \tilde{E}^*(v)\tilde{E}(v + \mu)e^{i2\pi(v+\mu)\tau} \\ &\quad + \tilde{E}(v)\tilde{E}^*(v + \mu)e^{-i2\pi(v+\mu)\tau} \rangle, \\ &= \Phi^{(1,1)}(v, v) + \Phi^{(1,1)}(v + \mu, v + \mu) \\ &\quad + \Phi^{(1,1)}(v, v + \mu)e^{i2\pi(v+\mu)\tau} \\ &\quad + \Phi^{(1,1)}(v + \mu, v)e^{-i2\pi(v+\mu)\tau}, \end{aligned} \quad (4.5)$$

where the Φ terms without subscripts describe statistics of $E(t)$, the envelope of interest. The envelope $P(t)$ is assumed to be cycloergodic with the result that the spectrometer measurement converges as

$$\begin{aligned} D(v; \tau, \mu, l', L', L) \\ \rightarrow_{L, L'} \begin{cases} W(v; 0) + W(v + \mu; 0) + W(v; m)e^{i2\pi(v+\mu)\tau} \\ \quad + W(v + \mu; -m)e^{-i2\pi(v+\mu)\tau}, & \mu = m\nu_T, \\ W(v; 0) + W(v + \mu; 0), & \mu \neq m\nu_T, \end{cases} \end{aligned} \quad (4.6)$$

where m is an integer. Note that the Hermitian symmetry of $\Phi^{(1,1)}(\nu_1, \nu_2)$ results in the relation

$$W(v; m) = W^*(v + m\nu_T; -m), \quad (4.7)$$

which ensures that Eq. (4.6) describes real-valued data. Non-negativity can also be proven using the inequality

$$|W(v; m)| \leq \sqrt{W(v; 0)W(v + m\nu_T; 0)}. \quad (4.8)$$

As shown in Eq. (4.6), the nonlinear SPIDER technique can be used to create a dependence between the $\nu_1 \neq \nu_2$ spectral correlations of $E(t)$ and measured data. This is evidenced by the $W(v; m)$, $m \neq 0$ terms that are present when μ is a multiple of the repetition rate ν_T .

With a well-chosen delay τ and band-limited $W(v; m)$ terms, the SPIDER data can be manipulated using linear filtering and demodulation to isolate a single term [42] and remove the dependence on τ . Assuming that $\mu = m\nu_T$, the processed data are

$$D'(v; m, l', L', L) \rightarrow_{L, L'} W(v; m). \quad (4.9)$$

The full $\Phi^{(1,1)}(\nu_1, \nu_2)$ spectrum may be constructed via Eq. (2.5) by taking measurements for multiple values of m . The resulting spectrum could then be used to characterize the stability of the source. For example, a nonstationary modal expansion [20,21] can be used to determine a nonstationary degree of coherence.

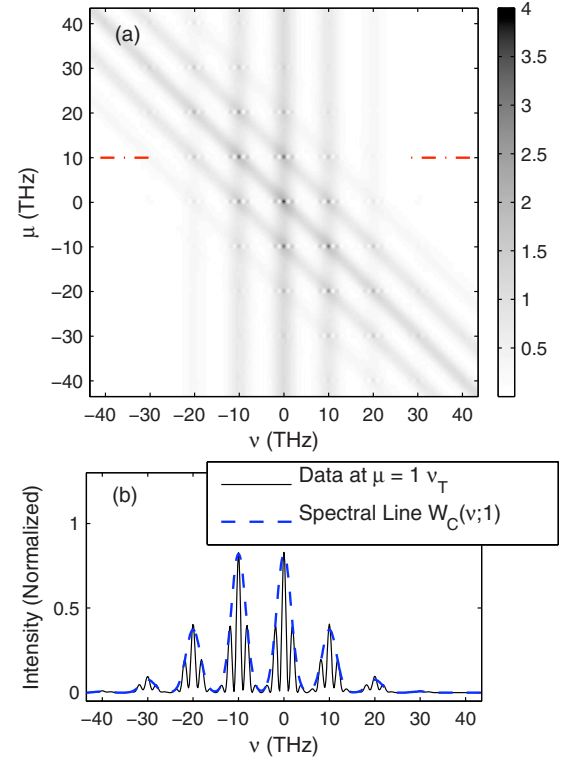


FIG. 4. (Color online) SPIDER data for the pulsed example field: (a) spectral profiles for many different spectral shears μ , plotted as an image, and (b) a single profile at $\mu = \nu_T = 10$ THz [marked with a dashed line in (a)], normalized by the maximum data value and plotted with the corresponding cross-spectral profile $W_C(v; 1)$.

The SPIDER data expected from the example signals described in Sec. II B can be calculated. The SPIDER data for the pulsed field (with spectrum shown in Fig. 1) can be seen in Fig. 4, while the stationary field (with spectrum shown in Fig. 2) gives the SPIDER data shown in Fig. 5. As dictated by Eq. (4.6), oscillatory spectral interference effects occur whenever the shear frequency μ is a multiple of the repetition frequency ν_T and the corresponding $W(v; m)$ term is nonzero. Consequently the pulsed field (Fig. 4) can be distinguished from the stationary field (Fig. 5) even though they have the same frequency content. Furthermore, the nonstationary spectrum seen in Fig. 1 can be estimated by measuring a full range of spectral shears.

The use of the SPIDER apparatus proposed here is significantly different from the traditional single-pulse, deterministic measurement scheme. In the deterministic case only a single spectral shear μ is required to calculate a spectral phase. However, a deterministic single-pulse measurement will not capture the statistical properties of the source. The stochastic case has a much greater range of potential measurements and as a result requires a multiple-shear measurement system. The construction of a multiple-shear SPIDER system may include significant technical hurdles and will ultimately be limited by the range and accuracy of shears μ that can be implemented. Additionally, the SPIDER implementation shown in Fig. 3 relies on temporally localized pulses. A stochastic field may be cyclostationary but not ex-

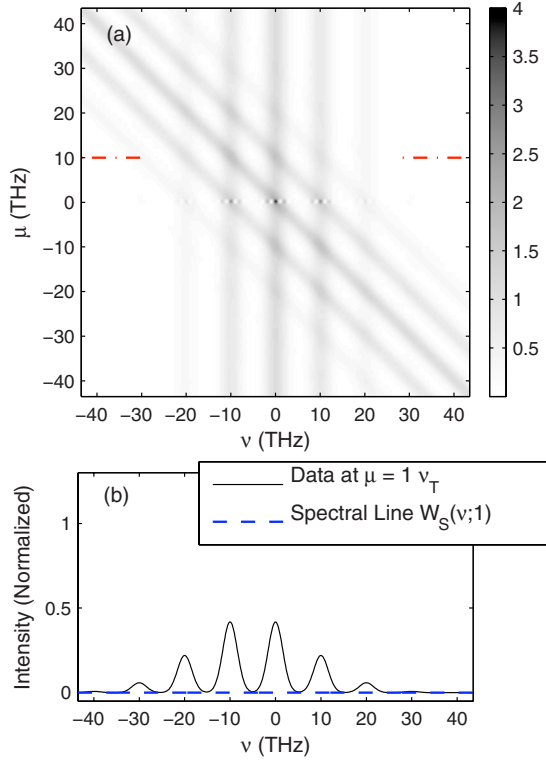


FIG. 5. (Color online) SPIDER data for the stationary example field: (a) spectral profiles for many different spectral shears μ , plotted as an image, and (b) a single profile at $\mu = \nu_T = 10$ THz [marked with a dashed line in (a)], normalized by the maximum data value and plotted with the corresponding cross-spectral profile $W_S(\nu;1)$.

hibit temporal localization. Despite these limitations, the analysis presented here illustrates the principle of nonstationary coherence measurements. There is also the possibility of utilizing a novel nonlinear and/or nonstationary instrument or other pulse measurement systems such as the FROG technique discussed in the next section.

C. Frequency-resolved optical gating

Like SPIDER, the ultrafast measurement technique FROG is used to measure the temporal profile of optical pulses [61]. FROG encompasses a family of measurement systems that depend on the optical arrangement and nonlinearity used. One example is second harmonic generation (SHG) FROG, which is illustrated in Fig. 6. SHG FROG can be cast in the framework used in Sec. IV B but with the predetector field

$$P(t; \tau) \propto E(t)E(t - \tau). \quad (4.10)$$

The Fourier transform of the predetector field $\tilde{P}(\nu; \tau)$ is then given by a convolution operation which can be written explicitly as

$$\tilde{P}(\nu; \tau) = \int \tilde{E}(\nu - \nu') \tilde{E}(\nu') e^{i2\pi\nu'\tau} d\nu'. \quad (4.11)$$

From the above result, the second-order spectral correlations of $P(t)$ can be calculated as

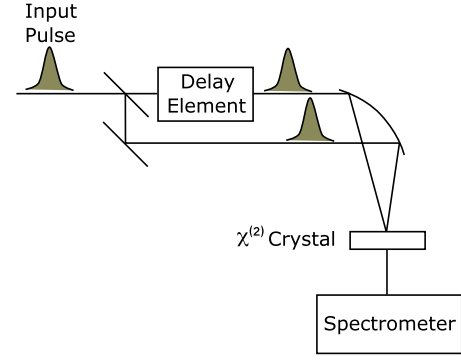


FIG. 6. (Color online) Illustration of the second-harmonic generation FROG technique. Two offset pulses are mixed in a nonlinear crystal and the resulting field detected with a spectrometer.

$$\begin{aligned} \Phi_p^{(1,1)}(\nu_1, \nu_2; \tau) &= \iint \Phi^{(2,2)}(\nu_1 - \nu', \nu', \nu' + \nu'', \nu_2 - \nu' - \nu'') \\ &\quad \times e^{-i2\pi\nu''\tau} d\nu' d\nu''. \end{aligned} \quad (4.12)$$

The second-order spectrum of $P(t)$ can be seen to be dependent on the fourth-order spectrum of $E(t)$, the field to be measured. This is because the FROG predetector field [Eq. (4.10)] is dependent on the product of $E(t)$ with a delayed version of $E(t)$; i.e., it is second-order in $E(t)$.

Due to cyclostationarity, the fourth-order temporal correlations of $E(t)$ are also periodic with respect to the placement of the time origin. Analogous to Eq. (2.5), this introduces a constraint on the form of the spectral correlations,

$$\begin{aligned} \Phi^{(2,2)}(\nu_1, \nu_2, \nu_3, \nu_1 + \nu_2 - \nu_3 + \mu) &= \sum_{m=-\infty}^{\infty} V(\nu_1, \nu_2, \nu_3; m) \delta(\mu - m\nu_T). \end{aligned} \quad (4.13)$$

Substituting Eq. (4.13) into Eq. (4.12) confirms that the second-order spectrum of the predetector data, $\Phi_p^{(1,1)}(\nu_1, \nu_2)$, is of the form given in Eq. (2.5), as required for a cyclostationary signal. Assuming the cycloergodicity of $P(t)$, the FROG data then converge as

$$\begin{aligned} D(\nu; \tau, l', L', L) &\rightarrow \iint_{L, L'} V(\nu - \nu', \nu', \nu' + \nu''; 0) \\ &\quad \times e^{-i2\pi\nu''\tau} d\nu' d\nu''. \end{aligned} \quad (4.14)$$

The integral in ν'' can be recognized as an inverse Fourier transform. As a result, the data can be more compactly represented by taking the Fourier transform with respect to τ , to give

$$\tilde{D}(\nu; f, l', L', L) \rightarrow \iint_{L, L'} V(\nu - \nu', \nu', \nu' + f; 0) d\nu'. \quad (4.15)$$

The forward model for the many-period SHG FROG system is given by Eq. (4.15). It can be seen that the fourth-order

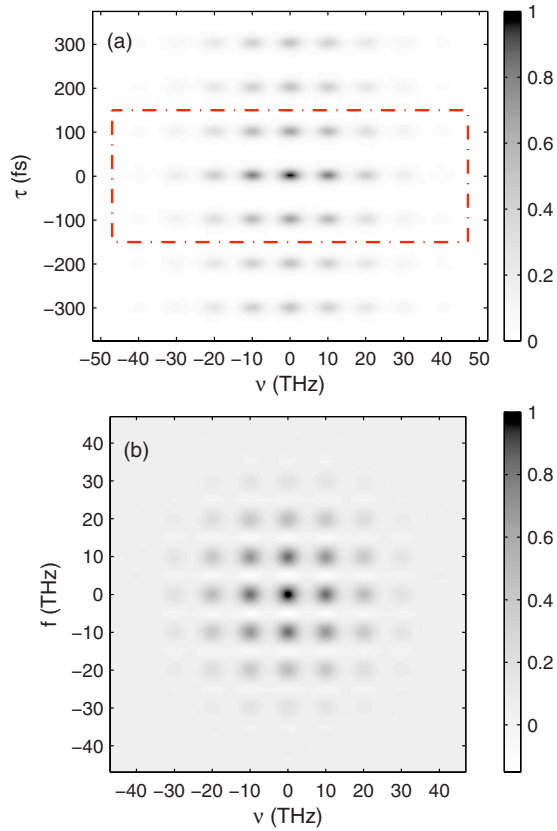


FIG. 7. (Color online) SHG FROG data for the pulsed example field: (a) data in the frequency and delay ($\nu-\tau$) domain and (b) data in the frequency and delay frequency ($\nu-f$) domain. To calculate (b) a one-dimensional Fourier transform was applied to the area within the dashed box in (a). The data in both (a) and (b) have been normalized.

statistics, determined by $V(\nu_1, \nu_2, \nu_3; m)$, are mapped to a two-dimensional data set. This gives a loss of dimensionality and hence an ill-posed inverse problem. However, the fourth-order spectral correlations can be expressed in terms of the second-order spectral correlations when the field $E(t)$ is statistically Gaussian (see Ref. [2] Sec. 8.5.3). Specifically,

$$\begin{aligned} \Phi^{(2,2)}(\nu_1, \nu_2, \nu_3, \nu_4) &= \Phi^{(1,1)}(\nu_1, \nu_3)\Phi^{(1,1)}(\nu_2, \nu_4) \\ &+ \Phi^{(1,1)}(\nu_1, \nu_4)\Phi^{(1,1)}(\nu_2, \nu_3). \end{aligned} \quad (4.16)$$

Restricting attention to cyclostationary fields, Eqs. (2.5) and (4.13) can be substituted above to give

$$\begin{aligned} V(\nu_1, \nu_2, \nu_3; m) &= \sum_{m''=-\infty}^{\infty} W(\nu_1; m'')W(\nu_2; m-m'') \\ &\times \delta(\nu_3 - \nu_1 - m''\nu_T) + \sum_{m'=-\infty}^{\infty} W(\nu_2; m') \\ &\times W(\nu_1; m-m')\delta(\nu_3 - \nu_2 - m'\nu_T). \end{aligned} \quad (4.17)$$

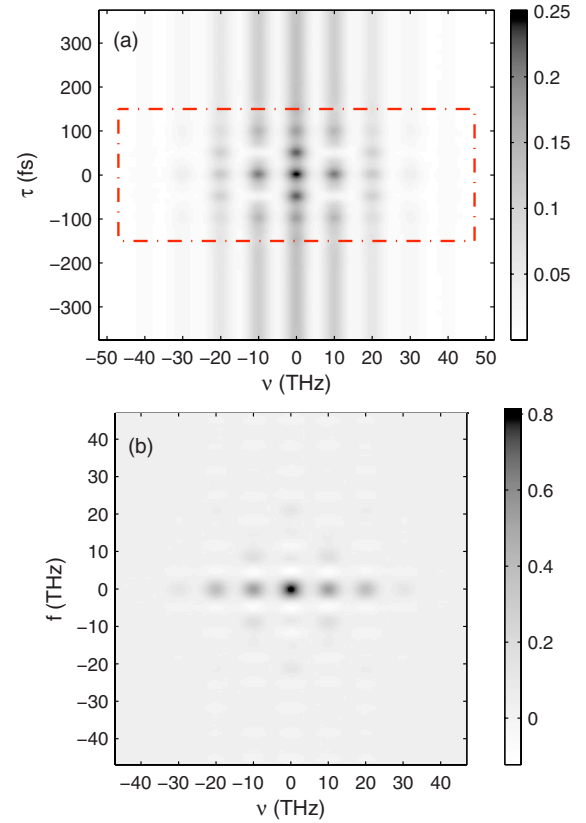


FIG. 8. (Color online) SHG FROG data for the stationary example field: (a) data in the frequency and delay ($\nu-\tau$) domain and (b) data in the frequency and delay frequency ($\nu-f$) domain. To calculate (b) a one-dimensional Fourier transform was applied to the area within the dashed box in (a). The data in (a) and (b) have been normalized to the same scale used in the corresponding plots in Fig. 7.

This relation can then be used in Eq. (4.15) and by making use of Eq. (4.7) it can be seen that

$$\begin{aligned} \tilde{D}(\nu; f, l', L', L) &\rightarrow \sum_{L, L' m=-\infty}^{\infty} \left[\int W(\nu'; m) \right. \\ &\quad \left. \times W^*(\nu - \nu' - m\nu_T; m) d\nu' \right] \delta(f - m\nu_T) \\ &+ \frac{1}{2} \sum_{m'=-\infty}^{\infty} W\left(\frac{\nu + f - m'\nu_T}{2}; m'\right) \\ &\quad \times W^*\left(\frac{\nu - f - m'\nu_T}{2}; m'\right). \end{aligned} \quad (4.18)$$

Like the SPIDER measurement [Eq. (4.6)], it can be seen that the SHG FROG instrumentation couples $W(\nu; m)$, $m \neq 0$ terms into the observable data. As a result, the nonstationary nature of the signal affects the data in a way not possible with linear, stationary measurements.

The first term in Eq. (4.18) is a weighted set of δ lines regularly spaced in f , corresponding to a periodic signal in τ . This periodic signal has the same repetition rate as the field and can be seen to arise from changes in the overlapping area

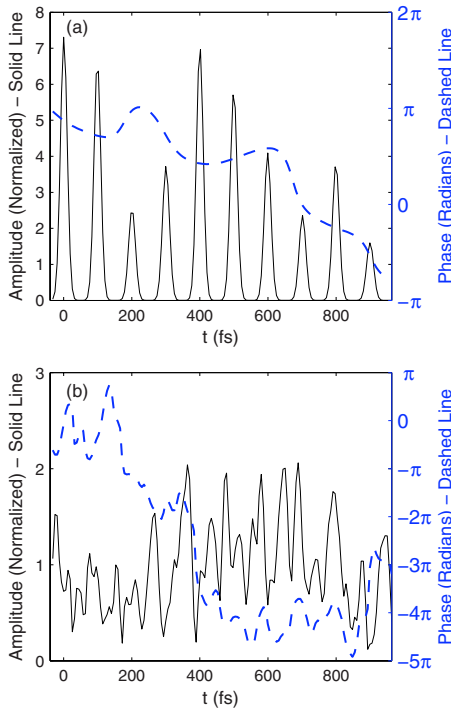


FIG. 9. (Color online) Realizations of (a) the pulsed example field and (b) the stationary example field. In both cases the amplitude scale is normalized to units of the mean amplitude. Note that the axis limits differ between (a) and (b) in both amplitude and phase.

of the two offset signals in Eq. (4.10). This term is periodic in τ and as such does not depend on the correlation length τ_c of $E(t)$, but rather on how energy is temporally distributed within a period T . Any effects of the correlation length [i.e., the range of τ over which $E(t)$ and $E(t-\tau)$ predictably interfere] enter the data through the second term in Eq. (4.18).

Figures 7 and 8 show SHG FROG data for the pulsed and stationary example fields described in Sec. II B. Since the SHG FROG data have infinite extent in τ , the effects of a finite data-collection window are significant. This is reflected in the figures, where the data window used to calculate the Fourier-domain data is shown. The windowing effect broadens and lowers the δ lines seen in Eq. (4.18) and also introduces some ringing artifacts. This can be seen by noting that for both example fields the expression given by Eq. (4.18) is non-negative, while negative values are seen in both Figs. 7(b) and 8(b).

The data from the stationary field seen in Fig. 8 are easily distinguished from those of the pulsed field seen in Fig. 7. However, unlike the SPIDER system, the FROG apparatus does not have a simple relationship between the data and the second-order spectral functions $W(\nu; m)$. In addition, a given data set does not uniquely determine a second-order spectrum, as can be seen by noting that a field with spectral components $W(\nu; \pm m)$ and a field with spectral components $e^{\pm i\phi_m}W(\nu; \pm m)$ produce the same data. Data interpretation is further complicated if the field statistics are non-Gaussian, as Eq. (4.15) must be used instead of Eq. (4.18). While the inverse problem of inferring the field statistics from SHG

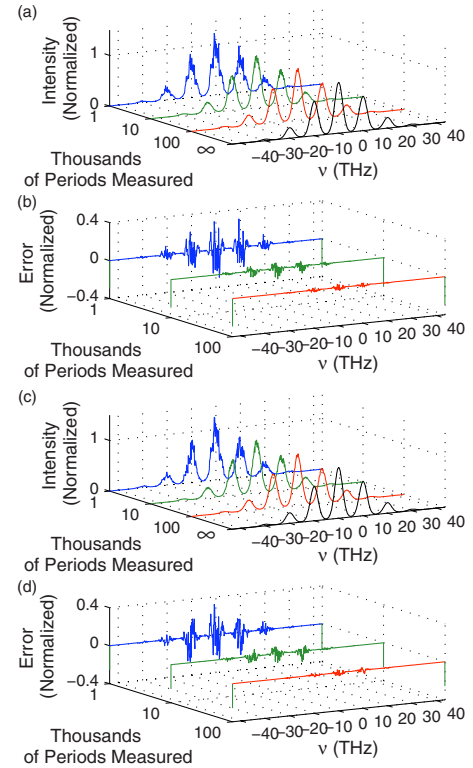


FIG. 10. (Color online) Computed spectra of the numerical examples: (a) spectra for time series of various durations and the predicted spectrum (marked with “ ∞ ”) for the pulsed field $E_C(t)$, (b) the differences between the measured spectra and the predicted spectrum for $E_C(t)$, (c) measured and predicted spectra for the stationary field $E_S(t)$, and (d) the differences between the measured spectra and the predicted spectrum for $E_S(t)$.

FROG data is neither trivial nor well posed, the ill-posedness may be mitigated by the inclusion of any prior knowledge of constraints on the source statistics. Alternatively, SHG FROG measurements may allow the estimation of incomplete but meaningful statistical metrics.

While data interpretation may be difficult with the SHG FROG system analyzed here, it does possess some important advantages over the SPIDER instrument. FROG can be experimentally realized in a robust instrument that has the capability of collecting both ν and τ simultaneously [62]. The SPIDER system described in Sec. IV B collects sequential one-dimensional data sets in order to construct two-dimensional data. The use of SPIDER systems also involves highly sensitive calibration procedures [63] that may have to be repeated for each shear μ measured. FROG may be limited by the length of delay τ that can be realized in the instrument, particularly if long-correlation-length fields are to be measured. However, the SHG FROG instrument shown in Fig. 6 does not rely on temporally localized pulses, in contrast to the SPIDER system seen in Fig. 3.

V. SIMULATIONS

In this section numerical simulations are used to demonstrate two results from the preceding theoretical work: that

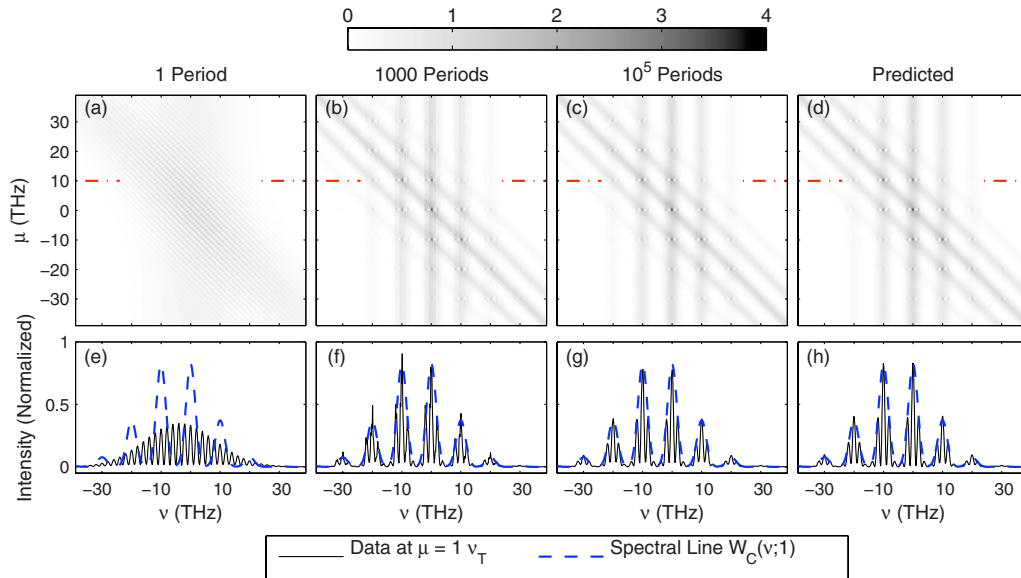


FIG. 11. (Color online) Computed SPIDER data for the pulsed field example: (a)–(c) normalized data as a function of frequency ν and shear μ for various field durations; (d) the predicted two-dimensional data; (e)–(g) one-dimensional profiles from the dashed position, $\mu = \nu_T$, in (a)–(c), scaled for comparison with the spectral profile $W_C(\nu;1)$; and (h) the predicted one-dimensional data.

the expressions describing stochastic many-period SPIDER and FROG data are valid and that the measurements converge as predicted by cycloergodicity. By manipulating the output of a Gaussian complex random number generator, time signals with prescribed stochastic properties can be generated [64]. These signals are then processed according to the measurement model, and the resulting signals are checked for convergence and consistency with the predicted data.

The two example fields described in Sec. II B are simulated. The stationary field $E_S(t)$ is realized by filtering the generated random numbers in a manner that takes white noise to a random process with the spectrum seen in Fig. 2. Similarly, the random numbers can be filtered in a manner that produces the spectrum shown in Eq. (2.9). The resulting time signal is then modulated according to Eq. (2.7) to produce a realization of $E_C(t)$. Examples of the realized fields can be seen in Fig. 9.

Despite clear differences in the time series of the pulsed and stationary fields, they have the same spectral energy distribution. This can be verified by defining a numerical spectrometer according to Eq. (3.7). The realizations of $E_C(t)$ and $E_S(t)$ were processed according to this spectrometer model, and the results are displayed in Fig. 10. Here the measurement duration L' is varied while L determines the spectral resolution, which in these examples is approximately 0.16 THz. From Fig. 10 it can be seen that both the pulsed and stationary examples converge to the same predicted spectrum. The close similarity of the spectra seen in Fig. 10, contrasted with the significant difference between the time plots seen in Fig. 9, further emphasizes the fact that measuring the power spectrum of a nonstationary field does not allow a characterization of the temporal statistics. The temporal statistics depend strongly on the frequency-to-frequency correlations. These $W(\nu, m)$, $m \neq 0$ terms describe the intermode correlation or, in the terminology of pulsed lasers, the mode locking.

Due to the stationary nature of $E_S(t)$ and the short period of $E_C(t)$, the instrument shown in Fig. 3 would not be suitable for measuring the example fields considered here. However, a hypothetical SPIDER measurement can be simulated by constructing the predetector field $P(t)$ according to Eq. (4.3). A delay of $\tau=500$ fs was used and the spectral shear μ was incremented in steps of approximately 0.77 THz. The resulting time series were each processed with the numerical spectrometer model. The results can be seen in Fig. 11 for the pulsed field and Fig. 12 for the stationary field. Again it can be seen that as the measurement duration is increased, the measured data converge to the predicted data. It should also be noted that when a single statistical period is measured, as in the traditional deterministic application of SPIDER, the resultant data are significantly different from those produced after many periods. In this work the SPIDER system is being used in a fundamentally different way—to characterize field statistics (e.g., period-to-period stability) rather than measure the field over a single period.

A SHG FROG simulation can be performed by constructing $P(t)$ from the realized time series according to Eq. (4.10) and then applying the computational spectrometer. The offset τ was incremented in steps of approximately 6.4 fs, and the resulting data can be seen in Fig. 13 for the pulsed field example and Fig. 14 for the stationary field example. The SHG FROG example also shows convergence and agreement with the theoretical prediction. Again, the single-period measurement differs substantially from the many-period, stochastic measurement.

VI. CONCLUSIONS

Motivated by pulsed lasers and sources driven by pulsed lasers, cyclostationary and cycloergodic models were applied to the measurement of stochastically periodic optical fields.

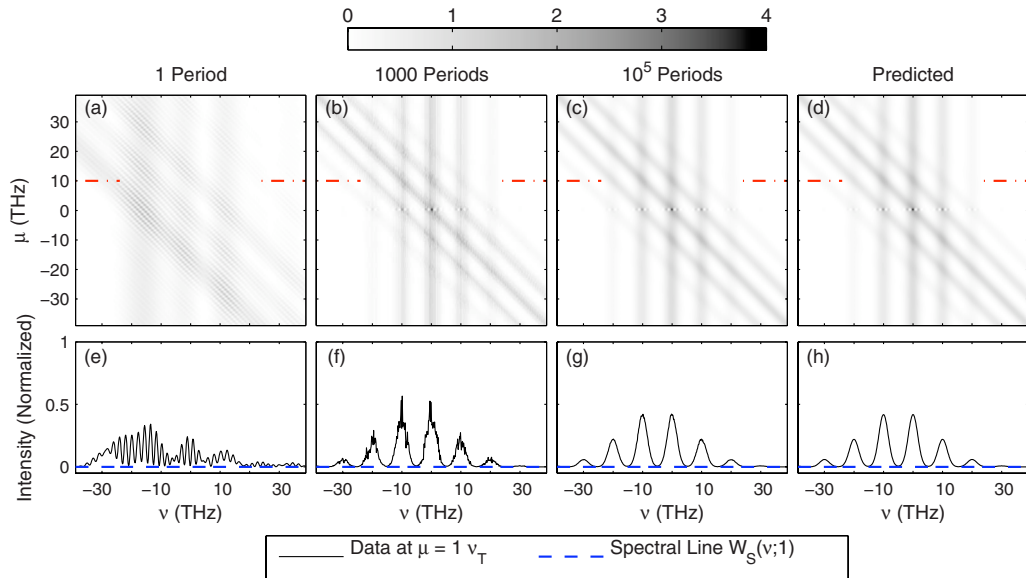


FIG. 12. (Color online) Computed SPIDER data for the stationary field example: (a)–(c) normalized data as a function of frequency ν and shear μ for various field durations; (d) the predicted two-dimensional data; (e)–(g) one-dimensional profiles from the dashed position, $\mu = \nu_T$, in (a)–(c), scaled for comparison with the spectral profile $W_S(\nu;1)$; and (h) the predicted one-dimensional data.

The resulting analyses generalize stationary ergodic coherence theory by including time-varying statistics and also contribute to nonstationary coherence theory by addressing ergodicity. That is, measurement precision is improved with increasing measurement integration times.

The second-order statistics of a nonstationary field are determined by the two-frequency correlation $\Phi^{(1,1)}(\nu_1, \nu_2)$. While linear, temporally stationary spectral measurements are only affected by $\nu_1 = \nu_2$ correlations, it was shown that nonlinear and/or nonstationary techniques such as SPIDER and FROG give data dependent on $\nu_1 \neq \nu_2$ correlations. Rather than applying these techniques in the standard manner—i.e., to characterize a single optical pulse—many-period measurements can be used to infer properties of the

spectrum $\Phi^{(1,1)}(\nu_1, \nu_2)$. Consequently, the stochastic many-period measurements have a meaning distinct from the deterministic single-pulse data.

It was seen that SPIDER can theoretically reconstruct the two-frequency spectrum completely while SHG FROG results in an ill-posed relation between the spectrum and the collected data. While the principle of statistical pulsed-source characterization has been demonstrated theoretically, current physical implementations of both SPIDER and SHG FROG may not be ideal for performing statistical measurements for all fields. In addition to investigating the performance of alternative existing ultrafast measurement technologies (e.g., [44,63]), further research may be done in the

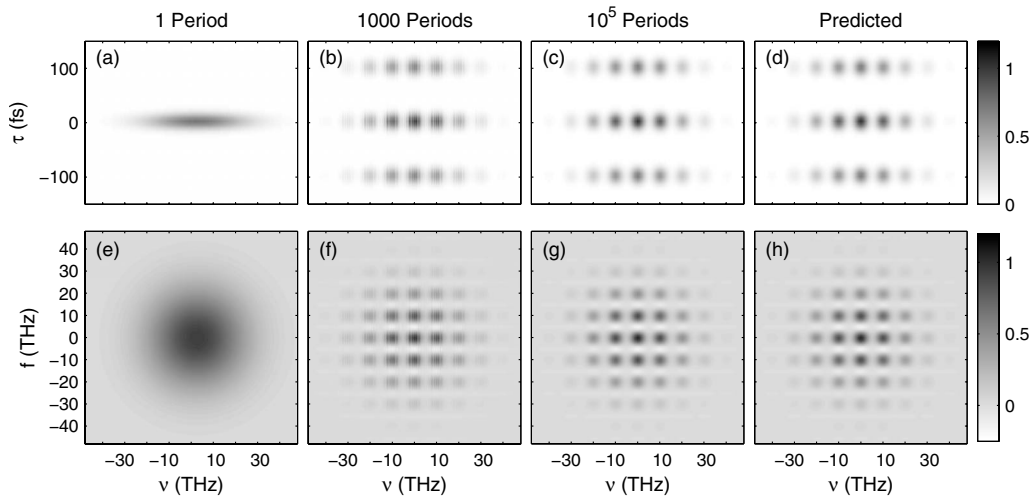


FIG. 13. Computed SHG FROG data for the pulsed field example: (a)–(c) normalized data in the frequency and delay ($\nu-\tau$) domain for various field durations, (d) the predicted $\nu-\tau$ domain data, (e)–(g) normalized data in the frequency and delay frequency ($\nu-f$) domain for the same set of field durations, and (d) the predicted $\nu-f$ data.

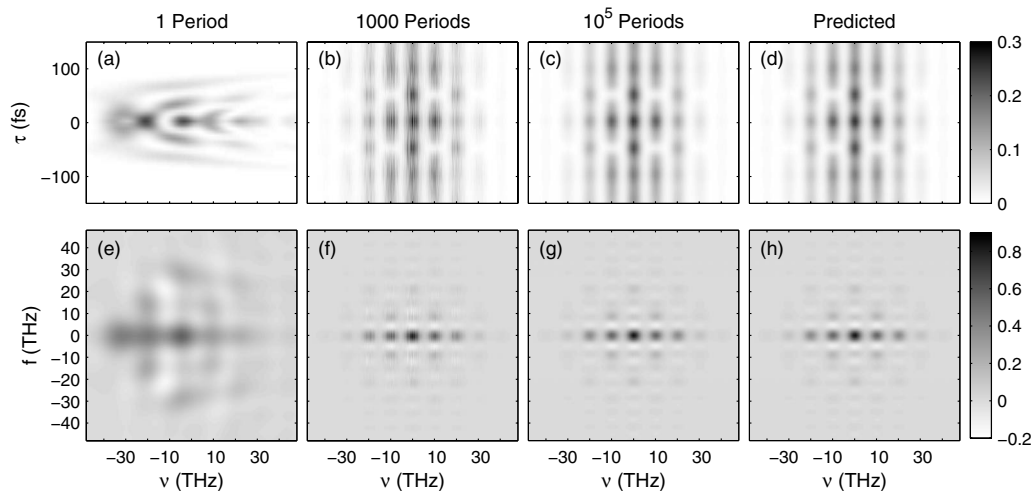


FIG. 14. Computed SHG FROG data for the stationary field example: (a)–(c) normalized data in the frequency and delay (ν – τ) domain for various field durations, (d) the predicted ν – τ domain data, (e)–(g) normalized data in the frequency and delay frequency (ν – f) domain for the same set of field durations, and (d) the predicted ν – f data. All data are normalized to the same scale used in Fig. 13.

development of novel instrumentation for the characterization of statistically pulsed sources.

The analysis presented here is independent of spatial position. The application of a cyclostationary model in the analysis of the spatiotemporal behavior of nonstationary fields may help connect theoretical predictions (e.g., [65]) and experimental results (e.g., [66,67]). It is also possible to relax the condition of cyclostationary statistics to almost-cyclostationary statistics [27], where the δ lines seen in the spectrum of Eq. (2.5) need not have a uniform spacing. This model could be used in the description of instruments that generate correlated modes at irregular frequencies (e.g., [37]). Finally, the work presented here may also be extended

to include the measurement of correlations between optical fields by, for example, using a many-period measurement in cross-correlation FROG [68].

ACKNOWLEDGMENTS

This work was supported in part by the Air Force Office of Scientific Research (Grant No. MURI F-49620-03-1-0379). The author would like to thank P. Scott Carney for valuable comments and criticism, and for continued support of this work. Robert W. Schoonover, Daniel L. Marks, and Rick Trebino are also acknowledged for helpful conversations.

-
- [1] J. W. Goodman, *Statistical Optics* (Wiley-Interscience, New York, 1985).
- [2] L. Mandel and E. Wolf, *Optical Coherence and Quantum Optics* (Cambridge University Press, Cambridge England, 1995).
- [3] C. Brosseau, *Fundamentals of Polarized Light: A Statistical Optics Approach* (Wiley, New York, 1998).
- [4] edited by J. Perina, *Coherence of Light* (Springer, New York, 1985).
- [5] J. H. Eberly and K. Wódkiewicz, *J. Opt. Soc. Am.* **67**, 1252 (1977).
- [6] R. Gase and M. Schubert, *Opt. Acta* **29**, 1331 (1982).
- [7] E. Wolf, *Phys. Rev. Lett.* **56**, 1370 (1986).
- [8] I. Newton, *Opticks: or, a Treatise of the Reflections, Refractions, Inflections and Colours of Light*, 4th ed. (William Innys, London, 1730).
- [9] L. C. Andrews and R. L. Phillips, *Laser Beam Propagation through Random Media* (SPIE Press, New York, 1998).
- [10] A. Labeyrie, *Astron. Astrophys.* **6**, 85 (1970).
- [11] D. Huang, E. A. Swanson, C. P. Lin, J. S. Schuman, W. G. Stinson, W. Chang, M. R. Hee, T. Flotte, K. Gregory, C. A. Puliafito *et al.*, *Science* **254**, 1178 (1991).
- [12] A. A. Michelson, London, Edinburgh Dublin Philos. Mag. J. Sci. **31**, 338 (1891).
- [13] A. A. Michelson, London, Edinburgh Dublin Philos. Mag. J. Sci. **34**, 280 (1892).
- [14] C. L. Mehta and E. Wolf, *Phys. Rev.* **157**, 1183 (1967).
- [15] R. Horák, *Opt. Acta* **16**, 111 (1969).
- [16] M. Bertolotti, A. Ferrari, and L. Sereda, *J. Opt. Soc. Am. B* **12**, 1519 (1995).
- [17] L. Sereda, A. Ferrari, and M. Bertolotti, *J. Opt. Soc. Am. B* **13**, 1394 (1996).
- [18] L. Sereda, A. Ferrari, and M. Bertolotti, *Pure Appl. Opt.* **5**, 349 (1996).
- [19] L. Sereda, A. Ferrari, and M. Bertolotti, *J. Mod. Opt.* **43**, 2503 (1996).
- [20] H. Lajunen, J. Tervo, and P. Vahimaa, *J. Opt. Soc. Am. A* **21**, 2117 (2004).
- [21] H. Lajunen, P. Vahimaa, and J. Tervo, *J. Opt. Soc. Am. A* **22**, 1536 (2005).
- [22] P. Vahimaa and J. Turunen, *Opt. Express* **14**, 5007 (2006).

- [23] A. T. Friberg, H. Lajunen, and V. Torres-Company, *Opt. Express* **15**, 5160 (2007).
- [24] H. Lajunen, J. Tervo, J. Turunen, P. Vahimaa, and F. Wyrowski, *Opt. Express* **11**, 1894 (2003).
- [25] R. W. Schoonover, B. J. Davis, R. A. Bartels, and P. S. Carney *J. Mod. Opt.* (to be published).
- [26] A. Papoulis and S. U. Pillai, *Probability, Random Variables and Stochastic Processes*, 4th ed. (McGraw-Hill, New York, 2002).
- [27] W. A. Gardner, A. Napolitano, and L. Paura, *Signal Process.* **86**, 639 (2006).
- [28] E. Serpedin, F. Panduru, I. Sari, and G. B. Giannakis, *Signal Process.* **85**, 2233 (2005).
- [29] I. G. Fuss, *IEEE J. Quantum Electron.* **30**, 2707 (1994).
- [30] O. Pottiez, O. Deparis, R. Kiyon, P. Mégret, and M. Blondel, *Opt. Lett.* **26**, 1779 (2001).
- [31] S. B. Cavalcanti, *New J. Phys.* **4**, 19.1 (2002).
- [32] B. Lacaze, *Opt. Express* **15**, 2803 (2007).
- [33] B. M. Sadler, *Appl. Opt.* **34**, 5091 (1995).
- [34] A. McPherson, G. Gibson, H. Jars, U. Johann, T. S. Luk, I. A. McIntyre, K. Boyer, and C. K. Rhodes, *J. Opt. Soc. Am. B* **4**, 595 (1987).
- [35] M. Drescher, M. Hentschel, R. Kienberger, G. Tempea, C. Spielmann, G. Reider, P. B. Corkum, and F. Krausz, *Science* **291**, 1923 (2001).
- [36] Y. Ozeki, S. Takasaka, J. Hiroishi, R. Sugizaki, T. Yagi, M. Sakano, and S. Namiki, *Electron. Lett.* **41**, 1048 (2005).
- [37] S. Zaitso, C. Eshima, K. Ihara, and T. Imasaka, *J. Opt. Soc. Am. B* **24**, 1037 (2007).
- [38] J. K. Ranka, R. S. Windeler, and A. J. Stentz, *Opt. Lett.* **25**, 25 (2000).
- [39] W. J. Tomlinson, R. H. Stolen, and C. V. Shank, *J. Opt. Soc. Am. B* **1**, 139 (1984).
- [40] X. Gu, L. Xu, M. Kimmel, E. Zeek, P. O'Shea, A. P. Shreenath, R. Trebino, and R. S. Windeler, *Opt. Lett.* **27**, 1174 (2002).
- [41] C. Iaconis and I. A. Walmsley, *Opt. Lett.* **23**, 792 (1998).
- [42] C. Iaconis and I. A. Walmsley, *IEEE J. Quantum Electron.* **35**, 501 (1999).
- [43] R. Trebino, K. W. DeLong, D. N. Fittinghoff, J. N. Sweetser, M. A. Krumbügel, B. A. Richman, and D. J. Kane, *Rev. Sci. Instrum.* **68**, 3277 (1997).
- [44] R. Trebino, *Frequency-Resolved Optical Gating: The Measurement of Ultrashort Laser Pulses* (Springer, Berlin, 2002).
- [45] Z. Y. Ou, G. K. Hong, and L. Mandel, *J. Opt. Soc. Am. B* **4**, 1574 (1987).
- [46] M. Bertolotti, L. Sereda, and A. Ferrari, *Pure Appl. Opt.* **6**, 153 (1997).
- [47] M. Bertolotti, A. Ferrari, and L. Sereda, *J. Opt. Soc. Am. B* **12**, 341 (1995).
- [48] G. Magyar and L. Mandel, *Nature (London)* **198**, 255 (1963).
- [49] V. Torres-Company, H. Lajunen, and A. T. Friberg, *J. Opt. Soc. Am. B* **24**, 1441 (2007).
- [50] R. A. Silverman, *IRE Trans. Inf. Theory* **3**, 182 (1957).
- [51] V. Devrelis, M. O'Connor, and J. Munch, *Appl. Opt.* **34**, 5386 (1995).
- [52] V. M. Papadakis, A. Stassinopoulos, D. Anglos, S. H. Anastasiadis, E. P. Giannelis, and D. G. Papazoglou, *J. Opt. Soc. Am. B* **24**, 31 (2007).
- [53] L. Lepetit, G. Chériaux, and M. Joffre, *J. Opt. Soc. Am. B* **12**, 2467 (1995).
- [54] I. A. Walmsley and V. Wong, *J. Opt. Soc. Am. B* **13**, 2453 (1996).
- [55] S. A. Ponomarenko, G. S. Agarwal, and E. Wolf, *Opt. Lett.* **29**, 394 (2004).
- [56] P. Pääkkönen, J. Turunen, P. Vahimaa, A. T. Friberg, and F. Wyrowski, *Opt. Commun.* **204**, 53 (2002).
- [57] H. A. Haus and A. Mecozzi, *IEEE J. Quantum Electron.* **29**, 983 (1993).
- [58] D. Eliyahu, R. A. Salvatore, and A. Yariv, *J. Opt. Soc. Am. B* **14**, 167 (1997).
- [59] R. Paschotta, A. Schlatter, S. C. Zeller, H. R. Telle, and U. Keller, *Appl. Phys. B: Lasers Opt.* **82**, 265 (2006).
- [60] C. Dorrer, B. de Beauvoir, C. Le Blanc, J.-P. Rousseau, S. Ranc, P. Rousseau, J.-P. Chambaret, and F. Salin, *Appl. Phys. B: Lasers Opt.* **70**, S77 (2000).
- [61] G. Stibenz, C. Ropers, C. Lienau, C. Warmuth, A. S. Wyatt, I. A. Walmsley, and G. Steinmeyer, *Appl. Phys. B: Lasers Opt.* **83**, 511 (2006).
- [62] P. O'Shea, M. Kimmel, X. Gu, and R. Trebino, *Opt. Lett.* **26**, 932 (2001).
- [63] J. R. Birge, R. Ell, and F. X. Kärtner, *Opt. Lett.* **31**, 2063 (2006).
- [64] B. J. Davis, *Opt. Express* **15**, 2837 (2007).
- [65] H. Lajunen, A. T. Friberg, and P. Östlund, *J. Opt. Soc. Am. A* **23**, 2530 (2006).
- [66] R. A. Bartels, A. Paul, H. Green, H. C. Kapteyn, M. M. Murnane, S. Backus, I. P. Christov, Y. Liu, D. Attwood, and C. Jacobsen, *Science* **297**, 376 (2002).
- [67] O. Jedrkiewicz, A. Picozzi, M. Clerici, D. Faccio, and P. Di Trapani, *Phys. Rev. Lett.* **97**, 243903 (2006).
- [68] S. Linden, H. Giessen, and J. Kuhl, *Phys. Status Solidi B* **206**, 119 (1998).